Journal of Structural Geology, Vol. 14, No. 8/9, pp. 1059 to 1077, 1992
Printed in Great Britain

0191-8141/92 $05.00+0.00
Pergamon Press Ltd

Deformation processes in eclogitic rocks: evidence for the rheological delamination of the oceanic crust in deeper levels of subduction zones*

PASCAL PHILIPPOT and HERMAN L. M. VAN ROERMUND

CNRS—URA 736, Laboratoire de Pétrologie Métamorphique, Université Paris 7, 4 place Jussieu, 75252 Paris Cédex 05, France

(*Received* 28 *October* 1991; *accepted in revised form* 15 *April* 1992)

Abstract—The deformation mechanisms and associated growth processes operating in omphacite during foliation development and veining have been studied in a km-scale eclogitic ductile shear zone from the Monviso meta-ophiolitic complex, Italian Western Alps. Dislocation creep due to multiple slip and/or climb is the dominant deformation mechanism, whereas (100) and (001) twinning, fracturing and intergranular fluid-phase diffusional creep are subordinate. Active slip systems include {110}[001], 1/2{110}⟨$\bar{1}$10⟩, (100)[001] and (1/2)(010)[100]. Fracturing is interpreted in terms of brittle instabilities arising from strain and pore fluid-pressure partitioning between adjacent omphacite domains. The transition from plastic to brittle behaviour of rocks is cyclic in nature as the internally generated fluids can be released and trapped repetitively during progressive deformation.

The significance of the eclogitic shear zone is discussed in terms of a mechanically weak zone that developed during burial or at least prior to the peak of temperature at a minimum depth of 40 km in a subduction zone, and which subsequently acted as a zone of detachment during a late stage of the Alpine orogeny. A rheological model for oceanic crust delamination in deeper levels of subduction zones is presented.

INTRODUCTION

DURING the last decade, several authors have used experimentally-determined flow laws for monomineralic rocks (halite, calcite, quartz, feldspar and olivine) together with recognition that the continental lithosphere is, to a good approximation, petrologically stratified, to infer that the lithosphere must exhibit substantial strength fluctuations with depth (rheological stratification; Ranalli & Murphy 1987, Rutter & Brodie 1988, Ord & Hobbs 1989). In addition, studies of naturally-deformed rocks have shown that a wide variety of factors other than rock type may have a strong control on the rheological behaviour of rocks of the lower crust and upper mantle. Among the most important factors (1) strain-induced progressive grain-size reduction during plastic flow (White 1976, Post 1977, Kirby & Kronenberg 1984, 1986), (2) metamorphic reactions (White & Knipe 1978, Rubie 1983, 1990a, Brodie & Rutter 1985), (3) pore-fluid pressure (Ismail & Murrell 1976), (4) changes in the dominant deformation mechanism (Rutter & Brodie 1988), or (5) intense crystallographic preferred orientations (Schmid & Casey 1986) may, independently or together, initiate de-stabilization of plastic flow into localized zones of high shear strain (i.e. strain-partitioning). The combination of rheological stratification and partitioning of deformation into localized ductile shear zones has led to the concept of crustal delamination (e.g. White & Bretan 1985). Such an interpretation is consistent with the common geological observation that cores of collision belts are characterized by the stacking of continental (and/or mantle) slices bounded by ductile shear zones.

The presence of mechanically weak zones has also been recognized in the oceanic lithosphere where it is thought to play a fundamental role in the emplacement of ophiolitic masses into arc–trench regions or collision belts (see Dewey 1976, Nicolas 1989 for a review). Two geodynamic environments are thought to be the sites for oceanic lithosphere delamination: (1) the oceanic ridge itself, where detachment of a thin oceanic lithospheric slab is initiated by decoupling along the lithosphere–asthenosphere boundary (Dewey 1976, Boudier & Coleman 1981) and (2) the trench axis of subduction zones, where bending of oceanic lithosphere entering the subduction zone can induce a shear fracture that propagates seaward (Nicolas & Le Pichon 1980, Van den Beukel 1990). Whatever the model considered, it is to be emphasized here that oceanic lithosphere delamination controlling detachment of lithosphere slabs is thought to occur at the ridge itself or in shallower levels of subduction zones. The question of to what extent rheological delamination is an important mechanism in the deeper levels of subduction zones (below 40 km depth) has received, paradoxically, little attention. This is probably due to the fact that prograde ductile shear zones or shear zones that formed prior to the peak of temperature are extremely rare in nature, thus preventing suitable studies of the deformation mechanisms operating during burial of eclogitic rocks.

In this paper, we present a detailed optical, universal stage and transmission electron microscopy (TEM) study of omphacite, the major framework-supporting mineral in eclogitic rocks, and describe the different deformation mechanisms operating in a well-preserved zone of high shear strain that formed during eclogite facies metamorphism. This study presents evidence for oceanic crust delamination at 40–50 km depth in a subduction zone environment.

*Contribution CNRS-INSU No. 469.

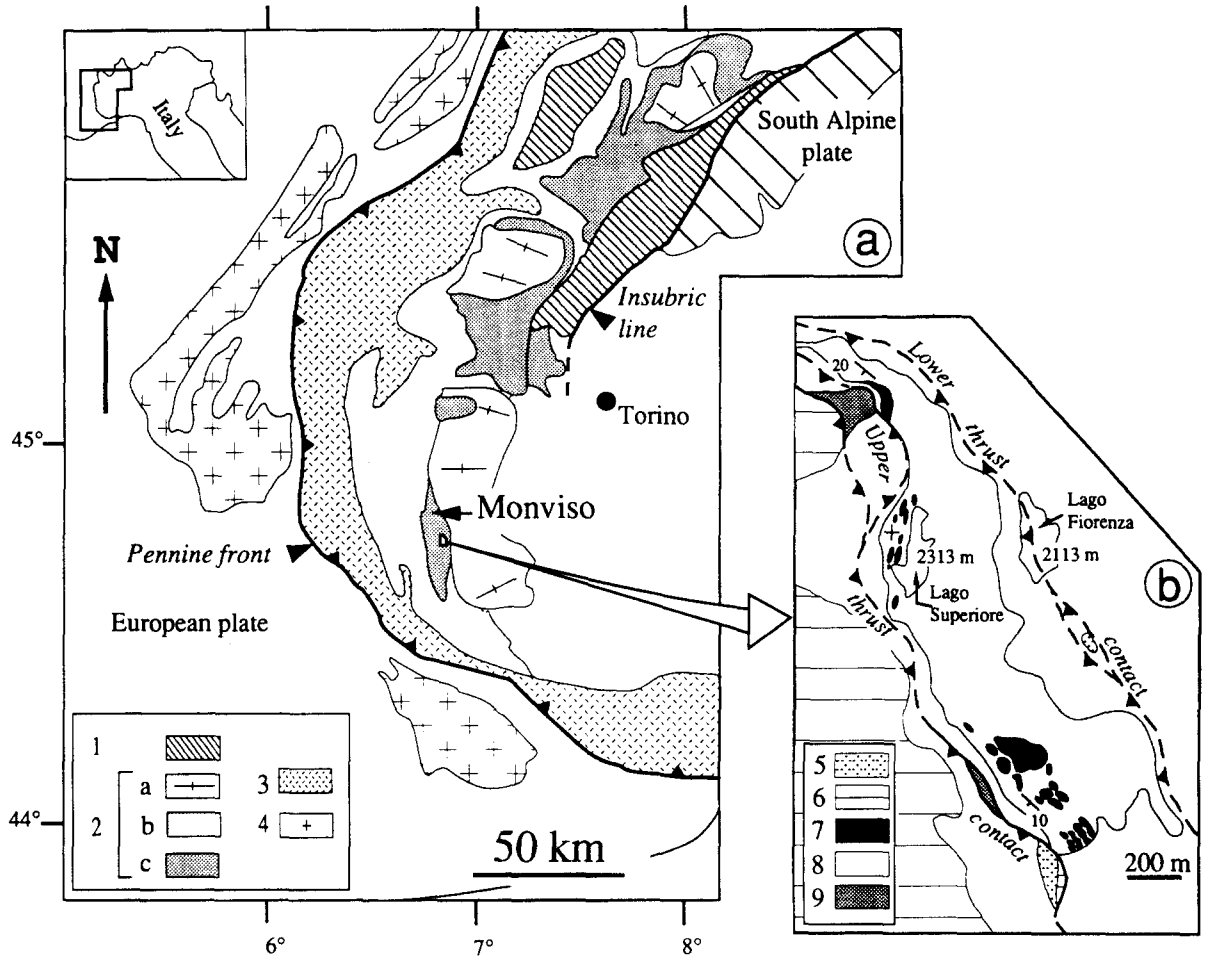

Fig. 1. (a) Schematic map of the Western Alps. 1, Austro-Alpine nappes. 2, Internal Pennine Zone, a, Internal Crystalline Massifs, b, schistes lustrés, c, main ophiolite complexes. 3, External Pennine Zone. 4, External Crystalline Massifs. (b) Schematic map of the Lago Superiore unit. 5, Calcschist. 6, Metabasalt. 7, Eclogite facies Fe-metagabbro. 8, Mg-metagabbro. 9, Serpentinite.

ECLOGITE FACIES METAGABBROS IN THE WESTERN ALPS

Eclogite facies metagabbros are well represented in meta-ophiolitic complexes of the Western Alps (Europe). The meta-ophiolites occur in two major nappes of the internal Pennine zone; the internal and external nappes of the schistes lustrés, respectively (Caby *et al.* 1978). These nappes surround the Internal Crystalline Massifs of the Pennine zone (Fig. 1a). The ophiolite bodies and associated sedimentary cover (schistes lustrés) are thought to represent remnants of one or several oceanic domains that separated the European and South Alpine continental margins during late Cretaceous (Elter 1971). Regional imprint of high-pressure metamorphism (Eoalpine event) in the Pennine zone has been used to support the suggestion of Cretaceous subduction (e.g. Dal Piaz *et al.* 1972), but recent studies (Monié & Philippot 1989) have determined a Mid-Eocene age for the Eoalpine metamorphism in the Monsivo meta-ophiolite body, thus emphasizing that the Eoalpine event in the Western Alps may be a much more long lasting event. In this paper, we have studied a major eclogitic ductile shear zone of the Monviso meta-ophiolitic complex in the Italian Western Alps (Fig. 1a).

MESOSTRUCTURES

The eclogite facies shear zone of this study is part of the Lago Superiore unit, which consists of a 2 km long and 200 m thick cumulate sequence of Mg- and Fe-rich metagabbros (Fig. 1b). This unit is bounded at the top and at the bottom of two late-stage tectonic contacts. The eclogitic rocks occur in the Fe-metagabbros that are located at the top of the cumulate sequence. The top of the cumulate sequence forms a 2 km long and 250 m large platform. The eclogitic rocks occur as large flat-lying boudins (10–100 m long, 5–100 m wide and 2–50 m thick) outcropping discontinuously over the entire platform, that is subparallel to the layering of the Fe-metagabbros. From these, we interpret the eclogitic boudins as remnants of a km-scale eclogitic ductile shear zone. The boudins of the eclogite facies shear zone are characterized by small volumes of low strain rocks (<1 volume% of the outcrop) preserving igneous textures that are surrounded by highly-deformed rocks

(mylonites, 95–98 volume%), which are in turn transected by different types of synkinematic veins (2–5 volume%). The low strain rocks, the mylonites and the veins, contain, in various proportions, the same omphacite, garnet, rutile and apatite eclogite facies mineral assemblage and show only local retrogressive alteration overprinting by blueschist and greenschist facies mineral assemblages. Within the mylonites, the shape preferred orientation of omphacite grains embedded in elongate domains of garnet and rutile aggregates define a clear plano-linear fabric, with a N–S stretching direction (Philippot 1988). These characteristics have been interpreted in terms of ductile–brittle deformation processes during eclogitic metamorphism (Philippot 1987). The roof tectonic contact lying above the eclogitic shear zone is marked by calcschists containing small bodies of metabasalts and serpentinites that were intensely deformed during subsequent retrograde blueschist and greenschist facies metamorphism; that is, during the rock exhumation history. The calcschists and metabasalts contain a pervasive foliation and an E–W-directed stretching lineation marked by strongly retrogressed blue amphibole, phengite, green amphibole, chlorite and albite. This implies that the roof thrust contact represents a late tectonic and kinematic feature with respect to the formation of the eclogitic shear zone. Temperature and pressure conditions of the eclogite facies metamorphism have been estimated at a minimum pressure of 10–12 kb and a temperature ranging between 450 and 550°C, by different authors using different methods (Lombardo *et al.* 1978, Kienast 1983, Lardeaux *et al.* 1986, Philippot & Kienast 1989).

MICROSTRUCTURES

Low strain rocks

Within the low strain rocks, the precursor igneous augite, plagioclase and Fe–Ti oxides occur fully pseudomorphed by an eclogite facies mineral assemblage; augite is mimetically replaced by 0.3–2 cm-large omphacite 1a crystals; plagioclase domains are pseudomorphed into a fine-grained aggregate (20–80 μm) consisting dominantly of omphacite 1b with minor amounts of zoisite and phengite; Fe–Ti oxides are mimetically replaced by 0.1–1 cm large rutile grains. In addition, original grain boundaries occur moted by 100–200 μm large solid inclusion-rich coronitic garnets (Fig. 2a). It is worth noting that omphacite 1a contains abundant fluid inclusions whereas omphacite 1b is fluid inclusion-free. Furthermore, both omphacite 1a and 1b have identical chemical compositions (Philippot & Kienast 1989).

Undulose extinction, twins, deformation and kink bands, healed fractures and a mantle of dynamically recrystallized new grains (omphacite 2) show that deformation processes affected the omphacite 1a megacrysts. In the pseudomorphed plagioclase domains, omphacite 1b occurs randomly oriented and equigranular to slightly elongated (with aspect ratios of 1:3). The omphacite 1b grain boundaries are irregular and generally straight to slightly curved. Triple-point junctions are common. The grains are optically strain-free, show only minor undulose extinction and do not contain intracrystalline subgrain boundaries. Locally, however, the pseudomorphed plagioclase sites form elongate lens-shaped domains that are tightly surrounding the omphacite 1a megacrysts. In these domains, omphacite 1b shows a marked shape preferred orientation and internal strain (undulose extinction), but neither recrystallization nor grain-size reduction has been observed. The grain boundaries are clearly irregular due to grain boundary migration. The boundaries between the adjacent omphacite 1b domains and the omphacite 1a megacrysts occur lined with thin layers of polycrystalline rutile (cm long) and discontinuous layers of fragmented solid inclusion-rich garnets. These are best interpreted in terms of fracturing of original rutile grains and corona garnets, and displacement of component fragments during foliation development (Philippot 1987). This heterogeneous and localized deformation associated with the omphacite 1b, the rutile and the garnet has important consequences for both the microstructural evolution and the rheology of the tectonite, and is discussed in more detail below.

Mylonites

In outcrop, the mylonitic domains exhibit a deformation pattern which is heterogeneous. Moderately to highly strained layers (1–10 cm thick) alternate and are parallel to the foliation plane. In the moderately strained domains, the precursor igneous texture, although still recognizable, is transposed parallel to the foliation plane resulting in a mm-scale layering (Fig. 2b). This layering is characterized by (1) relatively coarse-grained layers containing omphacite 1a megacrysts (severely reduced in size) in association with dynamically-recrystallized omphacite 2 (200–400 μm in size) that develop at the expense of omphacite 1a; and (2) fine-grained layers containing microcrystalline omphacite 1b (see the above description of the internal structure of the omphacite 1b domains in strained layers).

In the highly strained layers, microstructural relics of the precursor gabbro are completely obliterated by deformation (Fig. 2c). Dynamic recrystallization of omphacite 1a into omphacite 2 down to a grain size of 5 μm (with aspect ratios up to 1:20) has resulted in a marked elongate omphacite shape fabric parallel to the foliation plane. Omphacite 2 grain boundaries are highly irregular indicating that grain boundary migration processes have been activated. Intracrystalline omphacite 2 strain features include undulose extinction with minor subgrain boundary development. Fracturing of individual rutile grains into thin polycrystalline (2 μm) layers several centimetres in length (aspect ratios in excess of 1:100) provide the best marker of the foliation plane. Small (50–200 μm), solid inclusion-rich and irregularly-shaped garnets occur randomly distributed

throughout the highly strained layers. Owing to the small sizes of the omphacite 2 (mean value of 5 μm), omphacite 2 crystallographic preferred orientation (CPO) diagrams could not be produced by conventional universal stage techniques. However, optical observations suggest the [001] defines a maxima parallel to the lineation. This is consistent with omphacite CPO measured in other L-type eclogites (Helmstaedt *et al.* 1972). The chemical composition of the omphacite 2 is similar to the composition of the omphacite 1a and 1b (Philippot & Kienast 1989). Additionally, omphacite 2 grains are systematically fluid inclusion-free.

Annealed mylonites

Locally, optically strain-free and tabular omphacite 3 grains, up to a grain size of 600 μm, occur overgrowing the mylonitic fabric (Fig. 2d). Omphacite 3 grain boundaries are generally straight and regular; triple-point junctions are common. Associated garnets are equidimensional (100–400 μm), subhedral, frequently atoll-shaped and do not contain solid inclusions. The chemical compositions of the atoll-shaped garnets and the omphacite 3 are similar to the composition of the inclusion-rich garnets and the omphacite 1a, 1b and 2, respectively (Philippot & Kienast 1989). Locally, omphacite 3 contains fluid inclusions oriented parallel to the crystallographic faces of the grains and lining the overgrowth zones. Omphacite 3 microstructures are interpreted to represent annealed microstructures with concomitant grain growth driven by excess surface free energy. These annealed microstructures are similar to high-temperature (600–800°C) eclogites (Van Roermund & Boland 1981, Buatier *et al.* 1991), although the grain size is smaller. Two omphacite CPO diagrams related to the annealing/growth stage of omphacite 3 are shown in Fig. 6(a). These are characterized by [001] parallel to the foliation (S) with a strong maximum subparallel to the lineation (L), [010] parallel to S and normal to L, and [100] subperpendicular to S.

Veins

Two types of metamorphic veins have been recognized in the field: undeformed and deformed veins. Undeformed veins are oriented parallel to S and L, at an angle of 30–40° to S and L, or perpendicular to S and L (Fig. 3a). These have been interpreted in terms of shear and extensional fractures. Undeformed veins show a range of geometries and crystal morphologies including fibres, euhedral and tabular crystals, sector- and oscillatory-zoned omphacites. In the following we will refer to these different types of crystals as omphacite 4. Omphacite 4 contains abundant fluid inclusions; the size of the grains ranges between 0.2 and 4.5 mm with an average around 1–2 mm. Deformed veins contain different amounts of dynamically-recrystallized omphacite 5 grains that developed at the expense of omphacite 4 during progressive deformation, boudinage and/or fracturing of undeformed veins during ongoing mylonitization (Fig. 3b). The size of the omphacite 5 grains ranges between 500 and 800 μm; note that the size of omphacite 5 is significantly larger than the average grain size of omphacite 1b, 2 and 3 in the mylonites (20–80, 5–400 and 200–400 μm, respectively). Omphacite 5 does not contain fluid inclusion. In the studied veins, omphacite 4 and 5 show identical chemical composition to omphacite 1a, 1b, 2 and 3 (Philippot & Kienast 1989). The eclogitic veins primarily contain only omphacite; however locally, small amounts of garnet, rutile and/or apatite have also been observed (Philippot 1987).

Morphologically, the undeformed veins can be subdivided into two main subtypes. Type (1) veins have omphacite 4 extending continuously across the vein and occurring as syntaxial overgrowths on host omphacites located in the vein walls. These include crack–seal type of vein microstructure (Philippot 1987). Type (2) veins contain omphacite 4 that crystallized as independent crystals compared to the original wall rock grains and without optical continuity with them. These grains rarely cut across a vein from wall to wall, but most commonly occur randomly dispersed throughout the vein, hence precluding incremental strain path analysis. In some veins, small irregularly oriented omphacite 4 grains occur on the vein wall and are succeeded inwards by progressively larger grains that develop at the expense of their neighbours (Fig. 3a). These have been interpreted in terms of preferential growth of crystals with their [001] direction parallel to the incremental extension direction during succeeding periods of microcracking (Philippot 1987).

Omphacite CPO diagrams related to omphacite 4 in undeformed veins are shown in Figs. 6(b) & (c) (Fig. 6b refers to the vein of Fig 3a). A selective omphacite growth process is well illustrated in Fig. 6(b). Figure 6 (b-1) represents the CPO diagrams of small transitional omphacite grains located along the vein wall: [001] defines a clear maxima normal to the vein wall and [010] forms a girdle oriented parallel to the vein wall with a maxima corresponding to the intersection line between the vein wall and the external foliation plane (i.e. Y direction of the strain ellipsoid). In the coarse-grained omphacite crystals located toward the vein center, the [010] girdle is replaced by a marked [010] maxima parallel to the Y direction of strain ellipsoid, while [001] remains perpendicular to the vein wall (Fig. 6b-2). Omphacite 4 CPO diagrams constructed for an undeformed vein, that do not contain the transitional grains located along the vein walls (Fig. 6c), are similar to the fabric obtained for the coarse-grained crystals in Fig. 6(b-2).

Omphacite CPO diagrams performed in a deformed vein are shown in Fig. 6(d) (Fig. 6d refers to the vein of Fig. 3b). The vein is parallel to S and contains primary omphacite 4 crystals and dynamically-recrystallized omphacite 5 grains. Both types of omphacites show a preferred elongate shape orientation parallel to S and L measured in the surrounding mylonitic rock and are characterized by similar CPO diagrams: [001] lies

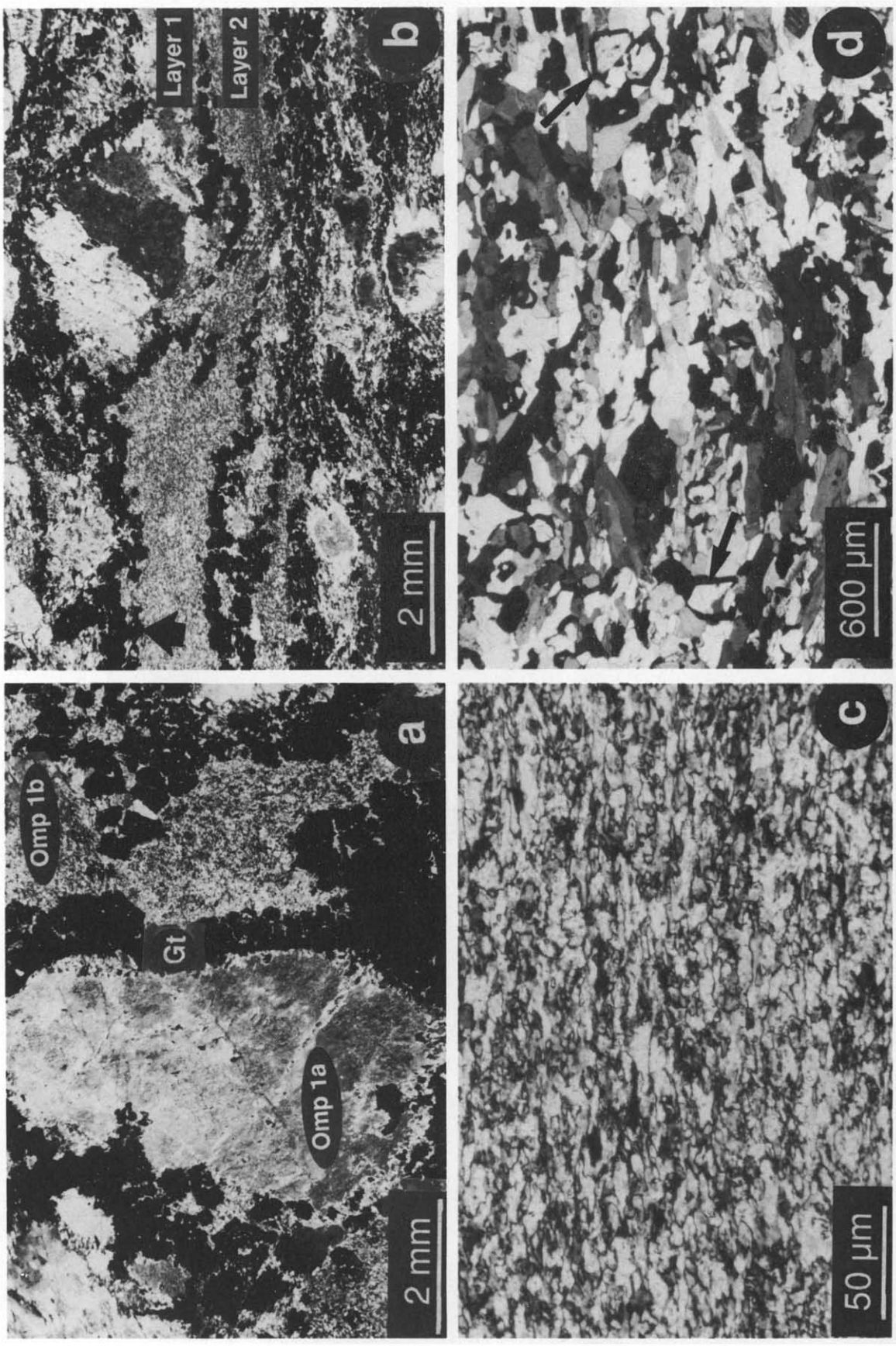

Fig. 2. (a) Microstructure of the low strain eclogitic rocks. Omp 1a: omphacite 1a megacryst mimetically overgrowing augite. Omp 1b: microcrystalline omphacite 1b filling the pseudomorphed plagioclase sites. Gt, corona of garnet. (b) Microstructure of the moderate strain domains. Layer 1 formed at the expense of omphacite 1a megacryst and contains residual omphacite 1a grains and dynamically-recrystallized omphacite 2 grains. Layer 2 contains microcrystalline omphacite 1b filling the pseudomorphed plagioclase sites. Note the layers of fragmented garnets (arrowed) lining the boundaries between layer 1 and 2. (c) Microstructure of dynamically-recrystallized omphacite 2 grains in a highly strained layer. Note the serrated grain boundaries (see text). (d) Microstructure of annealed domains. The arrows point to atoll-shaped garnets.

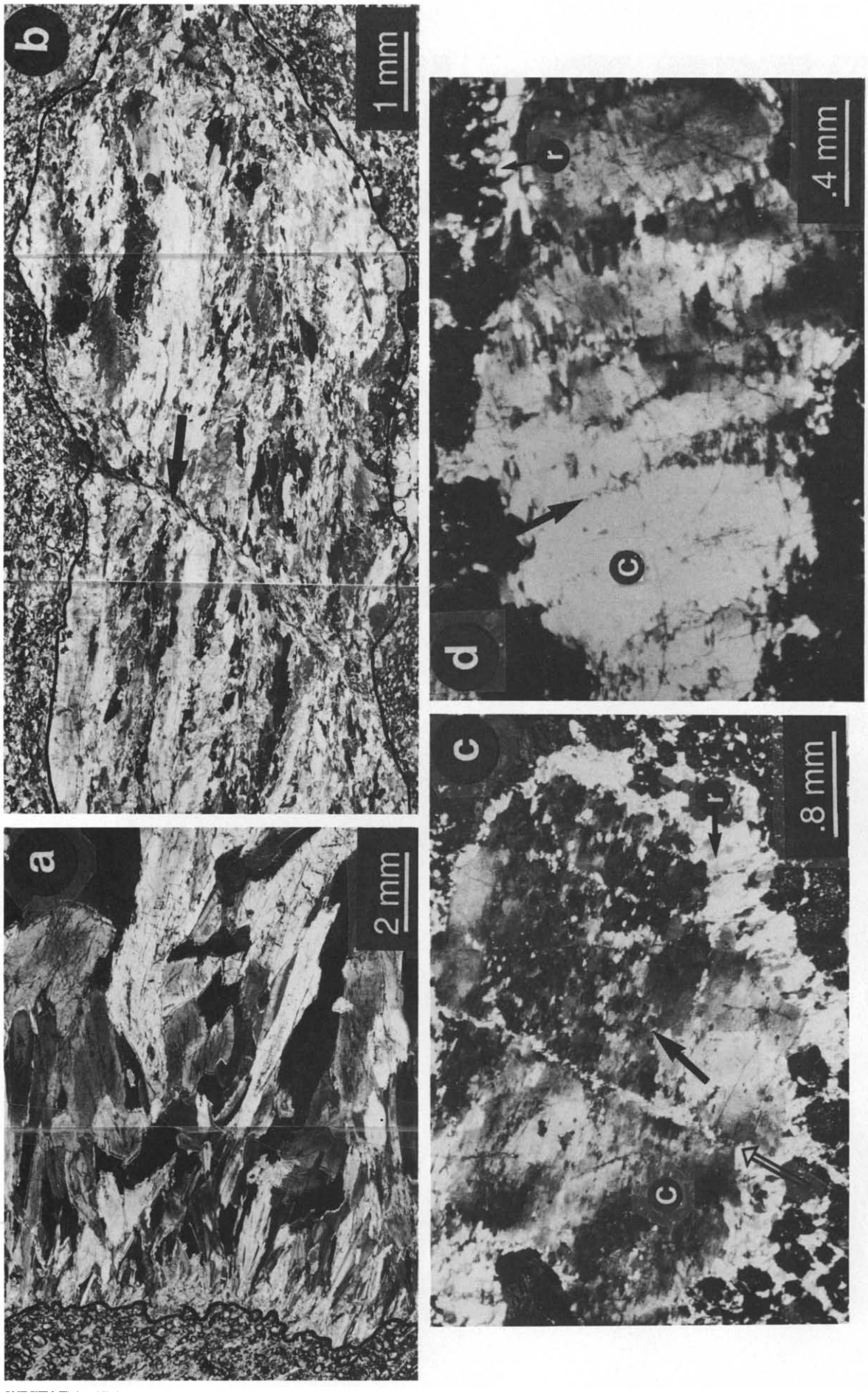

Fig. 3. (a) Undeformed omphacite vein. Small transitional omphacite 4 grains are located along the right-hand side of the vein wall (irregular line) and the large omphacite 4 fibres develop toward the vein centre. (b) Deformed omphacite vein lying parallel to the foliation plane. The arrow indicates a small shear band. (c) Subgrain geometry (blocky microstructure indicated by the black arrow) in an omphacite 1a megacryst (c = clast) mantled with dynamically-recrystallized omphacite 2 grains (r). Note the presence of an (001) kink (empty arrow). (d) (001) kink band microstructure (arrowed) in an omphacite 1a megacryst. The crystallographic relationship between the host and the new subgrains is shown in Fig. 9(a). Same labels as in (c).

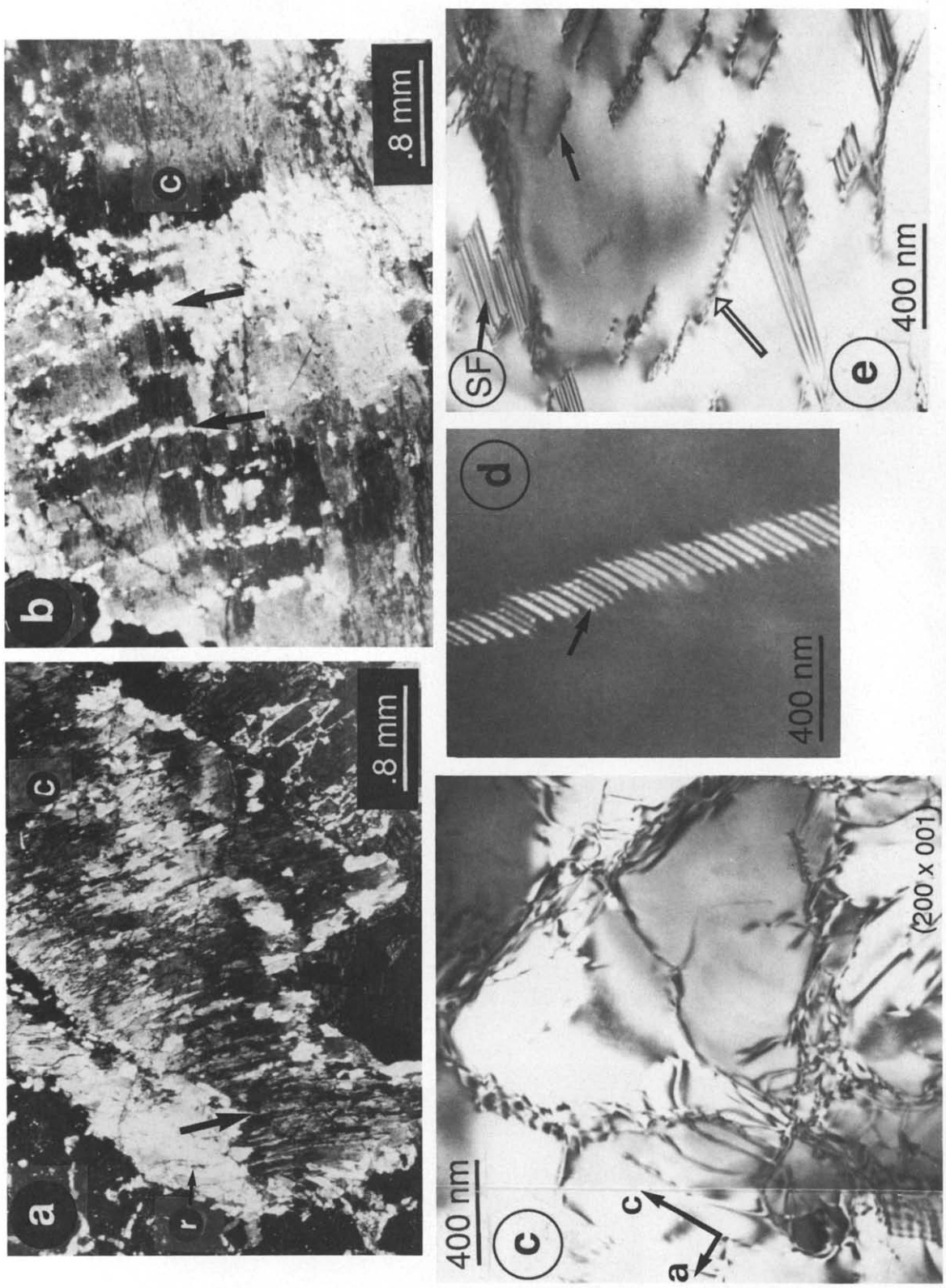

Fig. 4. (a) (100) twin (arrowed) in an omphacite 1a megacryst. The twin relationship is shown in the stereographic projection of Fig. 9(b). Migration of twin band boundaries resulted in the generation of subgrains (same legend as in Fig. 3c). (b) Trains (arrowed) of recrystallized new grains lining (001) twin bands in an omphacite 1a megacryst. The twin relationship between the clast and the recrystallized grains is shown in Fig. 9(c) (same labels as Fig. 3c). (c) Bright field electron micrograph illustrating the overall dislocation substructure (see text). Electron beam subparallel to [010], g = 001. (d) Dark field electron micrograph of a subgrain boundary by dissociated 1/2[100] dislocations (arrowed); g = 041. (e) Bright field electron micrograph of isolated [100] unit dislocations (black arrow) and dissociated 1/2[100] dislocations (empty arrow) separated by stacking faults (SF) of different width; g = 221.

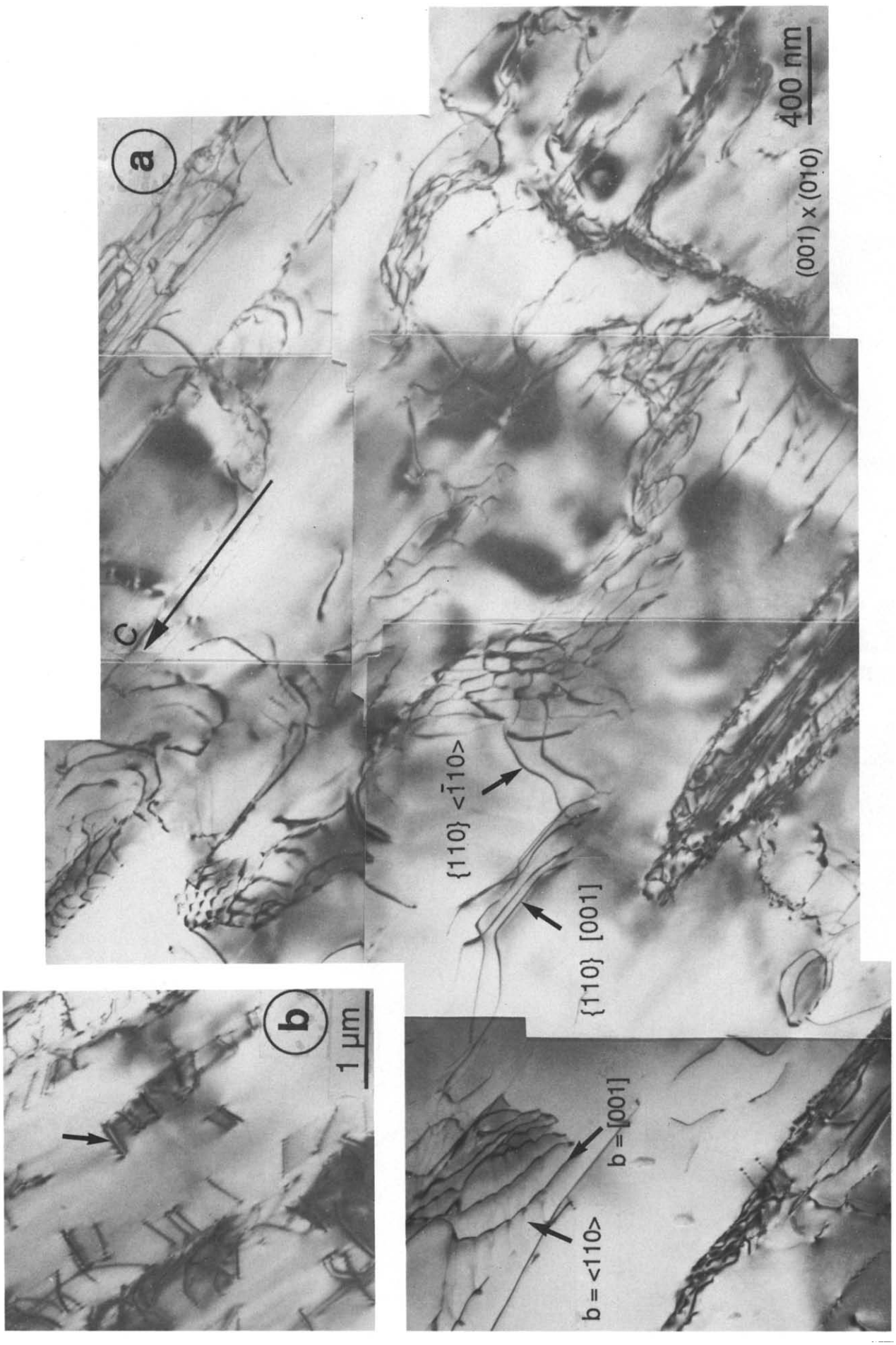

Fig. 5. (a) Bright field electron micrograph of dislocation substructure in an omphacite 1a megacryst containing isolated (010) subgrain boundaries at the optical scale. Electron beam subparallel to [100], $g = 001$. (b) Unit and partial [100] dislocations and associated stacking faults (arrowed) when sample is tilted around the [c] axis (c shown in a). Electron beam subparallel to [110], $g = 001$.

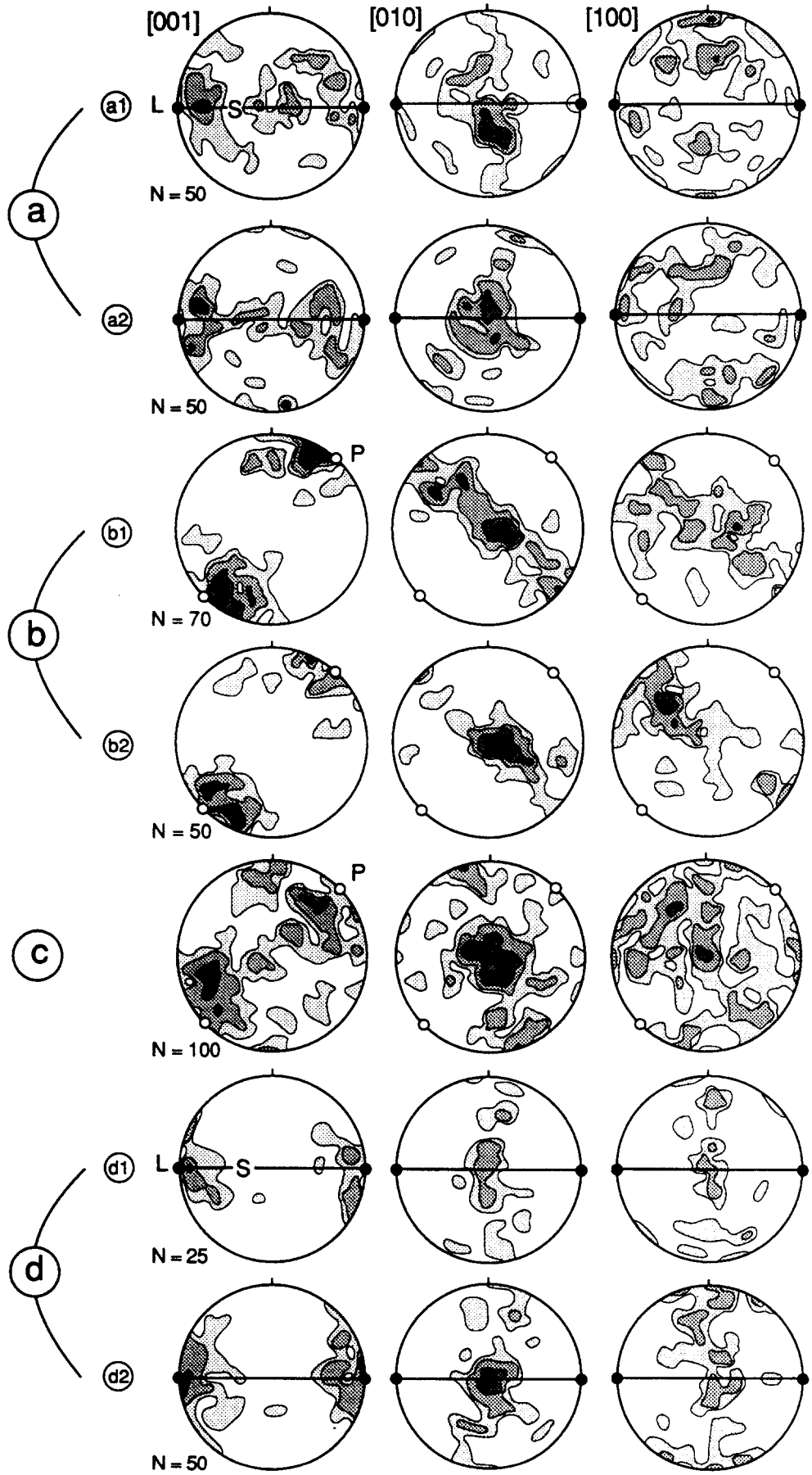

Fig. 6. Omphacite crystallographic preferred orientation (CPO) diagrams. L = stretching lineation direction, S = foliation plane and P = pole of the vein wall. (a) Omphacite 3 CPO diagrams in two annealed domains. Contours 0.5, 1, 2 and 3%. (b) Omphacite 4 CPO diagrams in the undeformed vein shown in Fig. 3(a). (b1) Small omphacite grains located on the vein wall. Contours 0.7, 1.4, 2.8, 4.2 and >5.6%. (b2) Large fibres located in the centre of the vein. Contours 0.5, 1, 2, 3 and >4%. (c) Omphacite 4 CPO diagrams in an undeformed vein containing only coarse grains. Contours, 1, 2, 4, 6 and >8%. (d) Omphacite CPO diagrams in the deformed vein shown in Fig. 3(b). (d1) Host omphacite 4 fibres. Contours 0.2, 0.5, 1, 1.5 and >2%. (d2) Dynamically-recrystallized omphacite 5. Contours 0.5, 1, 2, 3 and >4%.

parallel to S and L, and [010] and [100] form a girdle around L.

Fluid inclusion occurrence and composition

Omphacite 1a, 3 and 4 contain fluid inclusions in various abundances. In contrast, omphacite 1b, 2 and 5 are fluid-deficient. In omphacite 1a, the fluid inclusions occur randomly distributed throughout the crystals and show an elongated tabular shape parallel to the crystallographic [c] axis of grains. This suggests that the fluid inclusions filling omphacite 1a may be primary in origin. In the annealed domains, omphacite 3 contains small amounts of fluid inclusions oriented parallel to the crystallographic faces of the grains and lining the overgrowth zones. This argues for a primary origin of the fluid inclusions with respect to the recovery sequence. In omphacite 4, the fluid inclusions occur either in clusters located in the core of the grains, or as fluid inclusion bands lining the overgrowth zones of sector- and oscillatory-zoned pyroxenes. These textures undoubtedly argue for a primary origin of the fluids with respect to the veining stage (see Philippot & Selverstone 1991 for details).

Detailed microthermometric studies together with identification of the daughter minerals present in the different populations of fluid inclusions (using the Raman technique) show that the fluid filling the different types of inclusions are complex aqueous brines. The amount of fluids filling the low strain rocks and the veins is similar (0.2–0.3 wt% H_2O, Nadeau *et al.* in press). In contrast, only 0.05 wt% of fluids has been estimated in the mylonitic domains. The fluid inclusions can be subdivided into two major groups of grossly similar salinities and densities. Group 1 inclusions corresponds to the fluid inclusions filling omphacite 1a megacrysts. These show salinities of 17.6–21.2 wt% equivalent NaCl and densities of 0.96–1.03 g cm^{-3}. Group 2 inclusions include fluid inclusions in omphacite 3 and 4. These show salinities of 5–15 wt% equivalent NaCl and densities of 0.89–0.95 g cm^{-3}.

RESULTS

In the low strain domains, omphacite 1a megacrysts show several intracrystalline deformation features including undulose extinction, subgrains, isolated subgrain boundaries, twins, dynamically-recrystallized new grains and healed fractures. Commonly, several of these intracrystalline deformation features occur within one single megacryst.

Subgrains

In thin sections $\geq$30 μm thick, wavy undulatory extinction is widespread in omphacite 1a megacrysts. Lowering the thickness of the thin section down to 10 μm shows that the undulatory extinction is due to a marked fine-grained subgrain microstructure (Fig. 3c). Subgrains form the most prominent microstructure, have sharp optical boundaries generally subparallel to {110}, (100) and (010) and have an elongated shape parallel to [c]. Subgrain distribution is either heterogeneous or homogeneous throughout the host grain. Heterogeneously distributed subgrains occur as sharply delimited zones or bands of different shapes and sizes that locally cross-cut one another to form an anastomosing network. In contrast, homogeneously distributed subgrains form a checkered pattern throughout the entire host megacryst. In both cases the size of the subgrains ranges from 20 to 200 μm, with a dominant size range of 20–30 μm. Two representative universal stage analyses of the intracrystalline subgrain formation are shown in Figs. 7 and 8. Figure 7(a) shows a schematic graph of a microshear zone that develops within an omphacite 1a clast, while Fig. 8(a) illustrates a part of a checkered pattern. In both examples, universal stage measurements have been performed along traverses as indicated in Figs. 7(a) and 8(a). The results obtained indicate that the finite rotation axes between adjacent subgrains (or newly recrystallized grains) and host megacryst are widely scattered (Figs. 7b and 8b). In addition, the finite lattice rotations (Figs. 7c and 8c) and the subgrain rotation (Figs. 7d and 8d) are markedly heterogeneous both along a single traverse and adjacent traverses when compared.

Isolated subgrain boundaries

Isolated subgrain boundaries are less frequent and about two to three orders of magnitude larger than the type described above. Commonly, they occur cutting across an entire omphacite megacryst. Isolated subgrain boundaries are subparallel to (001), {110} and (010), with (001) being dominant. Universal stage measurements show that isolated (001) and {110} subgrain boundaries contain a rotation axis within the subgrain boundary plane. This rotation axis may be subparallel to [010], [001] or <110>, and remains constant in orientation when comparing parallel sets of isolated subgrain boundaries. This implies that isolated (001) and {110} subgrain boundaries can be interpreted in terms of simple kink band boundaries formed by single slip along (100)[001], {110}[001] or {110}<$\bar{1}$10>. In contrast, isolated (010) subgrain boundaries contain a pronounced twist component in the rotation axis oriented perpendicular to the subgrain boundary plane, thus implying that they formed by the operation of two or more slip systems. A representative example of complex (001) kink is shown in Figs. 3(d) and 9(a). Universal stage measurements indicate that the omphacite megacryst is kinked with kink band boundaries (KBB) subperpendicular to [001]. KBB rotation angles as well as KBB spacing vary significantly within the megacryst. In addition, KBB migration leading to serrated KBB, associated subgrain formation and/or recrystallization is common. Furthermore, adjacent KBB are commonly connected along the (100) planes by subgrain boundary

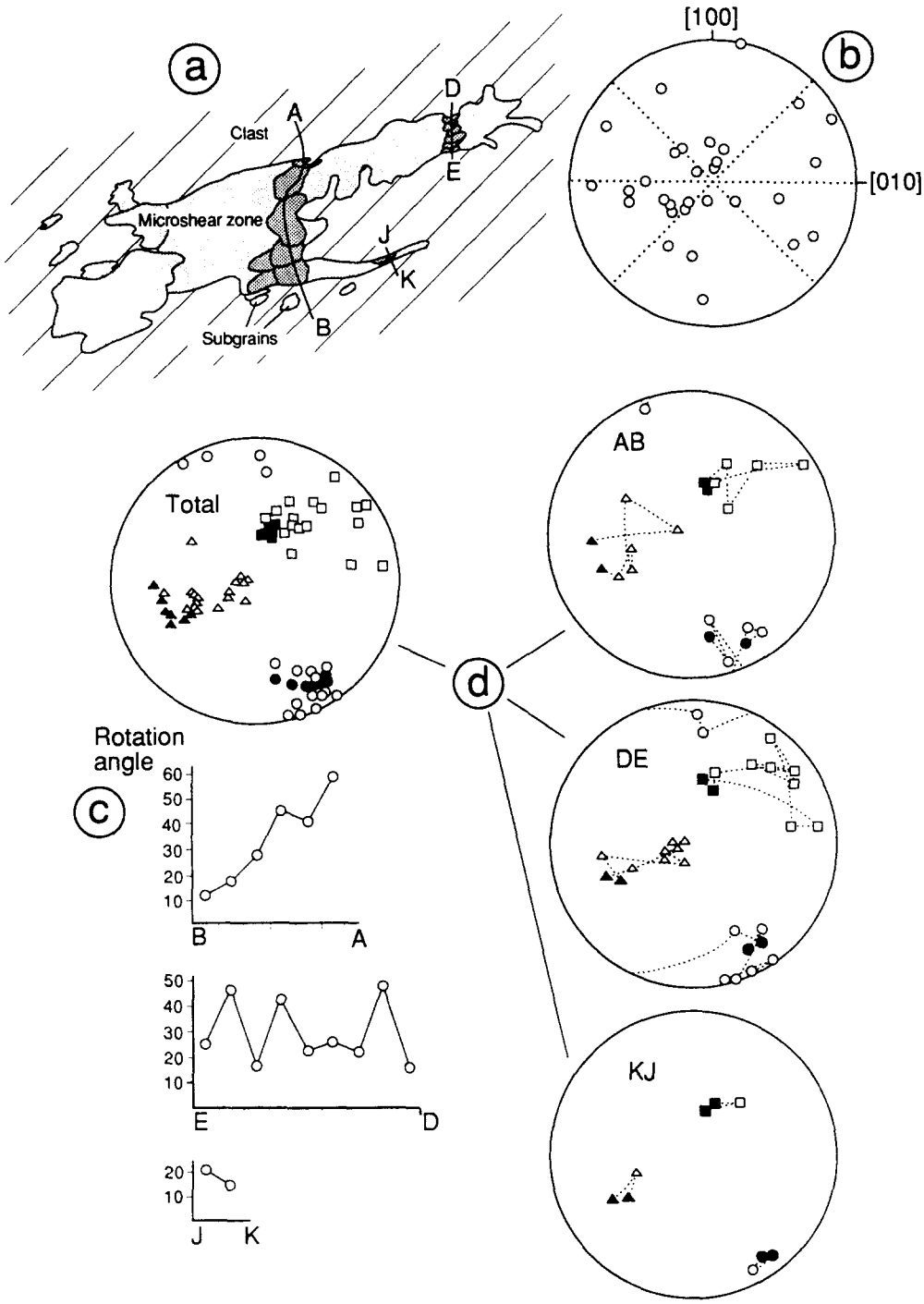

Fig. 7. Recrystallization mechanism analysis within an omphacite 1a megacryst showing heterogeneous subgrain distribution. (a) Drawing after microphotograph of a microshear zone. Trajectories along which universal-stage measurements have been performed are indicated. (b) Stereographic plot of all finite rotation axes measured between adjacent subgrains and host crystal. Reference frame represents the host crystal orientation and dotted lines characterize the possible slip systems. (c) Finite lattice rotation measured between adjacent subgrains along trajectories AB, DE and JK. (d) Stereographic plots showing the spread of subgrain misorientations measured along trajectories AB, DE and JK taken all together (Total) and separately. Black symbols = clast, empty symbols = subgrains, squares = [100], circles = [001], triangles = [010].

planes, (100) twin boundary planes or zones of newly recrystallized grains resulting in a blocky microstructure (Fig. 3d).

(100) *and* (001) *twins*

(100) and (001) deformation twins are common in omphacite 1a megacrysts, with (001) twins being, however, far less developed than the (100) twins (Figs. 4a & b and 9b & c). In addition, (100) and (001) twin band boundary (TBB) migration and associated recrystallization are common. In most cases, TBB migration and associated recrystallization have been so pronounced that the underlying deformation mechanism is completely obliterated. The original twin relationship between host and recrystallized grains can, however, still

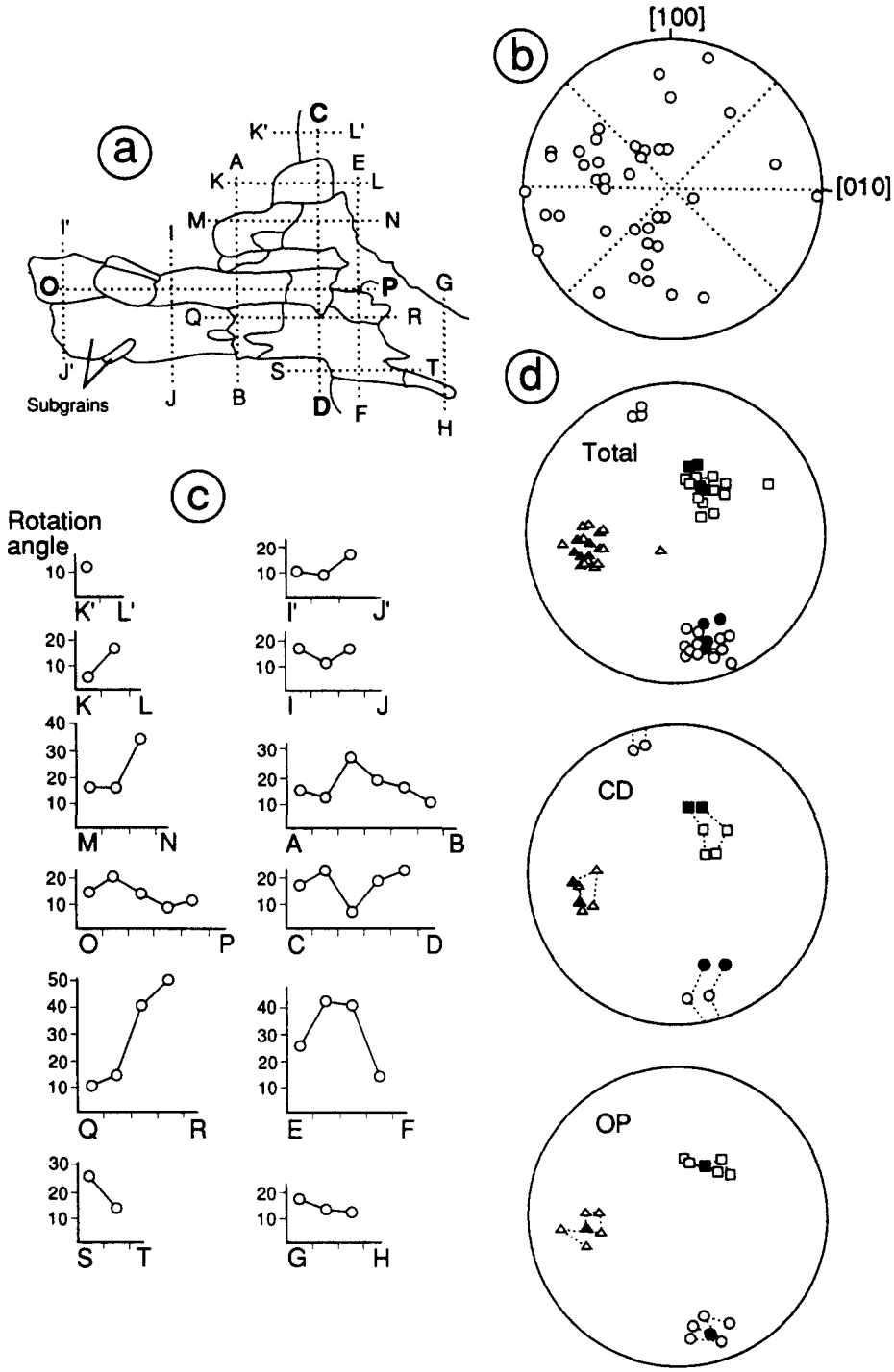

Fig. 8. Recrystallization mechanism analysis within an omphacite 1a megacryst showing homogeneous subgrain distribution. (a) Drawing after microphotograph of a part of a subgrain 'checkered' pattern. Trajectories along with universal-stage measurements have been performed are indicated. (b) Stereographic plot of all finite rotation axes measured between adjacent subgrains and host crystal. Reference frame represents the host crystal orientation and dotted lines characterize the possible slip systems. (c) Finite lattice rotation measured between adjacent subgrains and host crystal along each trajectory shown in (a). (d) Stereographic plots showing the spread of subgrain misorientations measured along the trajectories indicated in (a) taken all together (Total) and along trajectory CD and OP, respectively (symbols as in Fig. 7d).

be recognized by universal stage measurements; the sizes of the recrystallized grains produced by (100) twinning are one order of magnitude larger than those produced by subgrain rotation. In contrast, the sizes of the recrystallized grains produced by (001) TBB migration are similar to those produced by subgrain rotation.

Recrystallization

Omphacite 1a megacrysts occur in places mantled by a rim of optically strain-free omphacite 2 (Figs. 3c & d and 4a). The size of these recrystallized omphacite 2 grains is generally one order of magnitude larger (100–400 μm) than the size of the grains formed by an intracrystalline

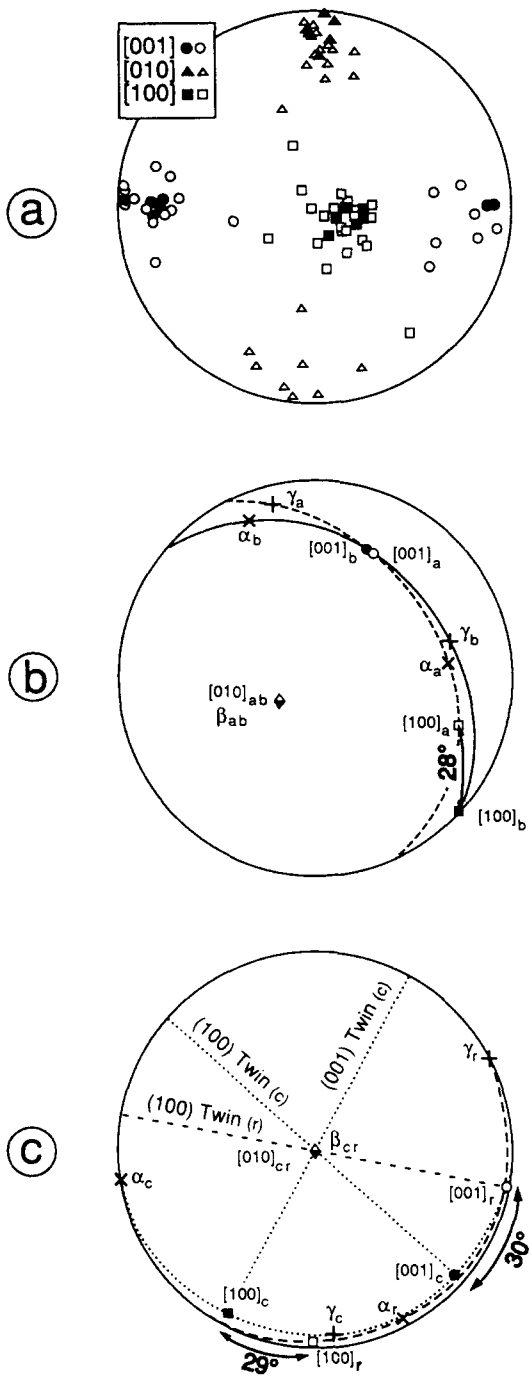

Fig. 9. (a) Stereographic projection of the (001) kink band microstructure of Fig. 3(d) showing the crystallographic relationship between the omphacite host (black symbols) and the dynamically-recrystallized grains (empty symbols). (b) Stereographic projection of the (100) twin shown in Fig. 4(a). Subscripts a and b refer to the subgrains developing along the twin band boundaries. (c) Stereographic projection of the (001) twin of Fig. 4(b) showing the twin relationship between the new intracrystalline grains (r) and the host crystal (c).

rotation-recrystallization mechanism. However, we were not able to study the recrystallization mechanisms operating in these grains since the sizes of omphacite 1b grains that develop in the adjacent pseudomorphed plagioclase sites were too small to analyse using conventional universal stage techniques.

TEM analyses

TEM analyses have been performed on omphacite 1a and 2. In all cases, TEM microstructures consist of a range of dislocation substructures and planar defects including (curved) free dislocations, loops, dissociated dislocations, tiltwalls, more complex dislocation networks, (100) and (001) twins and antiphase domains.

Most of the individual or free dislocations have Burgers vector [001] or 1/2<110>, the dissociated 1/2[100] dislocations being subordinate. The activated slip systems are (100)[001], {110}[001], 1/2{110}<$\bar{1}$10> with (1/2)(010)[100] being subordinate. [001] and/or 1/2<110> dislocations form the major component of tiltwalls and more complex dislocation networks. Well organized, generally complex subgrain boundaries delineating subgrain areas with a low dislocation density are the most predominant microstructure. Subgrain boundaries are commonly parallel to low index crystallographic planes (i.e. {110}, (100), (010) or (001)) or irrational and strongly curved (Fig. 4c). Except for some differences, this overall microstructure resembles the dislocation creep microstructure described by Van Roermund & Boland (1981) and Buatier *et al.* (1991). These differences are, in the present study: (1) smaller subgrain sizes (mean value of 20–30 μm), (2) the dislocation reaction [001] + 1/2<110> → 1/2<112> is generally absent in complex dislocation walls and/or intersection points between isolated [001] and <110> dislocations, (3) relics of relatively untangled dislocation networks are still locally present and (4) activation of the 1/2(010)[100] slip system.

The most common planar defects are antiphase domain (APD) boundaries. The sizes of the APD are systematically less than 500 Å. In addition, subordinate (100) and (001) twins, and (010) stacking faults occur. (010) stacking faults are abundant in samples containing isolated (010) subgrain boundaries. An overview of the dislocation substructures in such a sample is given in Fig. 5(a) in which B (=electron beam direction) lies parallel to the [100] direction. The dominant dislocation substructure consists in a complex dislocation network oriented subparallel to {110} with subordinate 'tiltwalls' oriented parallel to (001). Isolated [001] and <110> dislocations run subparallel to [001] or <110>, and truncated [001] and <110> loops characterize the slip directions in the {110} planes.

When the specimen is tilted along the [c] axis, trains of stacking faults lining up along (010) become visible (Fig. 5b). The stacking faults have highly variable width (≤700 Å) and are bounded by 1/2[100] dislocations. The line direction of the partial [100] dislocations is generally subparallel to [100] or [201]. However, although complex dislocation network involving [001] and [100] dislocations have not been observed parallel to (010), subgrains bounded by arrays of dissociated 1/2[100] dislocations are common (Fig. 4d). These subgrains show an elongate shape parallel to (010). They are interpreted to be due to a polygonization process involving (010)[001] slip. The formation of the stacking faults

most likely post-dated the polygonization process since locally, and within the resolution limits, [100] unit dislocations have been observed (Fig. 4e). However, the large spread in stacking fault-width probably indicates that (010) slip also occurred by migration of 1/2[100] partial dislocations.

Finally, a small number of isolated 1/2(010)[100] stacking faults have been observed in all analysed samples. This probably indicates that the (010)[100] and/or 1/2(010)[100] slip system has only a small contribution to the overall strain accommodated by omphacite. Because it is the first time that this slip system is reported in clinopyroxene, a more detailed and rigorous description will be published elsewhere (Van Roermund & Philippot in preparation).

Fluid origin and mass transport processes

In an attempt to address the problem concerning the origin of the fluids and the scale of mass transfer accommodating veining, detailed fluid inclusion and stable isotope studies have been performed by Philippot & Selverstone (1991) and Nadeau *et al.* (in press); some of their results are incorporated here in order to provide constraints on the model of fluid-rock mechanical interaction to be developed below.

The fact that the dynamically-recrystallized omphacite 2 and 5 are fluid-deficient indicates that the fluid inclusions present in omphacite 1a and 4, respectively, have been released during crystal plastic flow, to subsequently form an intergranular free fluid phase wetting the boundaries of omphacite 2 and 5 grains. Relics of such microstructures are preserved within the annealed omphacite 3 crystals. Indeed, recognition of fluid inclusions lining the overgrowth zones argues for fluid entrapment during omphacite 3 growth. The salinity and density differences recorded between group 1 (low strain rocks) and group 2 (annealed domains and veins) inclusions are probably partly due to trapping of different generation of inclusions at differing temperature and/or pressure. As discussed by Nadeau *et al.* (in press), group 1 inclusions filling omphacite 1a megacrysts probably represent a stage of entrapment predating group 2 inclusions entrapment in omphacite 3 and 4 (exsolution inclusions that precipitated from the host mineral during omphacite replacement of augite or from fluids derived from breakdown of hydrated minerals such as amphibole or chlorite). In the annealed domains and in the veins, the fluids have similar salinities and densities thus indicating that they were trapped under similar P–T conditions. This implies that periods of fluid releases and entrapment associated with crystal plastic flow and omphacite growth processes, respectively, are intimately related in time. Furthermore, estimates of the fluid content present in the different microstructural domains (0.2–0.3 wt% H_2O in the low strain rocks and in the veins, and about 0.05 wt% H_2O in the mylonites) show that the fluids liberated during crystal plastic flow were subsequently compensated by fluid entrapment in the veins.

Fluid inclusion and stable isotope analyses showed that fluid heterogeneities occurred on a mm-scale within a single vein (Philippot & Selverstone 1991) and that oxygen isotopic heterogeneities occurred on a cm-scale between adjacent veins and mylonitic layers (Nadeau *et al.* in press). This together with the fact that the veins and the mylonites contain identical mineralogies imply that the scale of fluid and isotopic equilibration was very small, thus arguing for short-range mass-transfer processes (cm-scale fluid-phase diffusional mass transport) rather than fluid infiltration over a relatively large scale leading to fluid and stable isotope equilibration. Furthermore, the lack of fluid and isotopic homogenization implies that fluid–rock interaction is best explained in terms of fluid generated internally to the eclogitic ductile shear zone.

SUMMARY AND INTERPRETATION

According to Knipe (1989), deformation mechanisms which can operate in rocks include diffusive mass transfer, crystal plasticity, grain boundary sliding as well as fracture and cataclasis. Following this classification, crystal plasticity is considered to be the dominant deformation mechanism operating in the eclogitic rocks studied, whereas fracturing and related fluid phase diffusive mass transfer processes are considered as subordinate. Optical and TEM studies showed that dislocation creep is accommodated by multiple slip (and climb) along {110}[001], 1/2{110}<$\bar{1}$10>, (100)[001] and (1/2)(010)[100], with (1/2)(010)[100], and (100) and (001) twins being subordinate. Specifically, recognition of (001) twins most probably reflects variations in strain rate during mylonization. In addition, the omphacite microstructures indicate that progressive deformation accommodated a switch in the dominant recrystallization mechanism from rotation-recrystallization in omphacite 1a megacrysts to migration-recrystallization in the highly strained layers. This is in marked contrast with the results obtained by Rubie (1990a, b) on similar rocks from the Sesia Lanzo Zone, Western Alps. Before developing a model for the rheological delamination of the oceanic crust in deep levels of subduction zones, it is worthwhile first considering an overview of the microstructural evolution and rheology of the eclogitic tectonites.

Microstructural evolution

Figure 10 illustrates a tentative model by which the spatial distribution and progressive evolution of the various microstructural domains described in this paper are explained by the progressive deformation of a single gabbroic body. In the low strain rocks, the omphacite 1a megacrysts and the microcrystalline omphacite 1b have identical chemical composition; this indicates that the metagabbros have completely equilibrated in the eclogite facies thus precluding studies of the kinetics and reaction pathways controlling eclogite formation. This

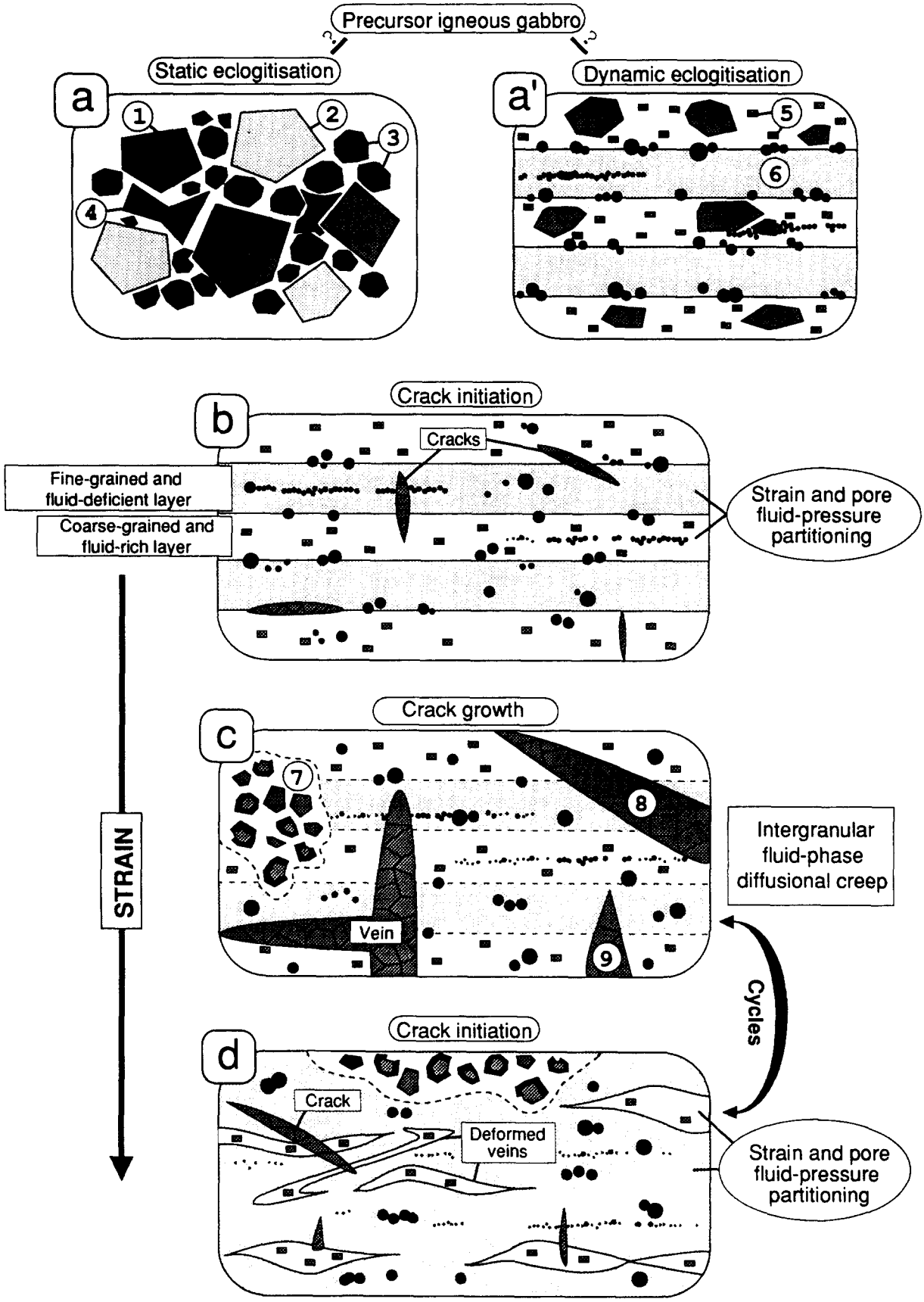

Fig. 10. Schematic diagram of the microstructural evolution of the eclogitic tectonites. (a) Low strain domain. 1, Omphacite 1a megacryst overgrowing augite. 2, Microcrystalline omphacite 1b filling pseudomorphed plagioclase site. 3, Garnet corona. 4, Rutile overgrowing ilmenite. (a') Moderate strain domain. 5, Dynamically-recrystallized omphacite 2 grains developing at the expense of omphacite 1a (coarse-grained layer). 6, Omphacite 1b fine-grained layer. (b) Moderate strain domain. (c) High strain domain. 7, Annealed domain. 8, Shear fracture. 9, Extensional fracture. (d) High strain domain (see text for discussion).

implies that we were unable to evaluate to which extent the gabbro to eclogite phase transition was completed: under static conditions (Fig. 10a) or enhanced by deformation processes (Fig. 10a').

Evidence for heterogeneous flow between adjacent microstructural domains can be seen in the low strain rocks where large omphacite 1a megacrysts generate intense crystal plastic flow in the adjacent microcrystalline omphacite 1b domains and fracturing of rutile and garnet. Although intracrystalline plastic processes including dislocation creep and climb have been active in omphacite 1a megacrysts, these domains are considered to be more resistant than the adjacent omphacite 1b domains during early stages of the deformation.

Ongoing deformation resulted in the superposition of 1 to several mm thick layers of different mineralogies, grain sizes and containing different amounts of free fluids. These observations have two important consequences on the microstructural evolution and the rheology of the tectonites.

(1) Pore fluid is most likely to have both a strong softening and an increase in ductility effects, either by facilitating diffusive mass transfer (White 1976) or by accelerating the emission and absorption of dislocations at grain boundaries (Rehbinder effect, see Rutter 1972). It is suggested that in the omphacite 2 domains, migration–recrystallization processes leading to a continual grain size reduction (down to a grain size of 5 μm) were greatly facilitated by the presence of a fluid film wetting the omphacite 2 grains. Accordingly, this suggests that at a given stage of the tectonic evolution, the omphacite 2 domains acted as zones of concentrated deformation.

(2) Pore fluid under pressure can significantly reduce the strength and the ductility of a rock by reducing the effective compressive stresses (Paterson 1978). In the omphacite 2 domains, high pore-fluid pressure could facilitate the opening of microcracks on a grain scale by reducing the fracture strength of the grain aggregate. However, this effect must have been counteracted to some extent by the increased crystal plasticity effect described above. In fact, both of these competitive effects could have been active in different domains or at different time depending on the ability of the rock to deform plastically at the imposed rate. From these we suggest that, in the moderately to highly strained domains, differences in grain size and in fluid content between adjacent omphacite domains may generate local strain and pore fluid-pressure partitioning; such rheological differences and fluid-pressure differences could have initiated microcrack development on a μm- to mm-scale (Fig. 10b).

Recognition of small-scale fluid and stable isotope heterogeneities shows that the eclogitic veins are best interpreted in terms of local segregation involving extremely short range mass transport. Therefore, the extension sites for the growth of material are not regarded as 'elongated cavities' created by crack propagation at one instant in time subsequently filled by a fluid phase. All that is needed is a continuous fluid film of sufficient thickness to allow flux of material through the fluid. With a wet fluid film we refer to the island-channel type of grain-to-grain contact described by Raj & Chyung (1981). In a non-hydrostatically stressed solid, in which grains occur in contact with one another and with a pore fluid, the diffusive mass transfer process is envisaged to occur via an interconnected free-fluid phase comprising dissolution of material at grain-to-grain contacts under high normal stress, solute diffusion through the intergranular fluid phase driven by a gradient in chemical potential (μ), and precipitation at interfaces under low normal stress such as the pore walls in the annealed domains or the vein walls. If local chemical equilibrium between solid and solute were to persist at all points of the island-channel type of grain-to-grain contacts, gradients in μ of the solute would exist and drive diffusive flux of solute from locations of relatively high μ to locations of relatively low μ (Spiers & Schutjens 1990, Schutjens 1991). This mechanism is known as grain boundary diffusional intergranular pressure solution (Weyl 1959); it assumes some kind of open grain boundary structure (island-channel type) capable of maintaining an interconnected fluid phase at the grain contacts. Therefore when such an interconnected fluid film forms on a local scale during ongoing deformation, continuous stress-enhanced dissolution and precipitation of omphacite (±garnet, rutile and apatite) would take place, while migration of the solute through the fluid film is driven by local chemical gradients in the pore fluid. This is clearly supported by the fact that, in the veins, the composition and salinity of the fluids are heterogeneous on a mm-scale.

Progressive opening of the fractures (locally indicated by crack–seal microstructures, Fig. 10c) is subsequently compensated by the growth rate of omphacite filling the crack. In this model, the volume amount of fluid needed is low (0.2–0.3 wt%) as the same fluid can be used repetitively. Furthermore, the occurrence of both undeformed and deformed veins indicate that the fluids that have been trapped in veins have been liberated several times during vein deformation. This implies that fracturing and associated fluid-phase diffusional mass-transfer process described above are cyclic in nature (Fig. 10d). Pockets of fluid used in early vein formation can be released again on a local scale during vein deformation and enhance the process elsewhere. Therefore, we suggest that such a transition from plastic to brittle behaviour is regarded as a self-perpetuating phenomena that may last until ductile deformation ceases.

Rheology

In terms of the rheological behaviour of the oceanic crust at eclogite facies conditions, an analogy can be made with the common interpretation that, in the middle and lower continental crust (i.e. aseismic zone), highly localized zones of high shear strain represent mechanically weak zones that accommodate motion between fragments of crust or lithosphere (e.g. White &

Bretan 1985). Such zones are recognizable because of the intense foliation development and grain size reduction present within them, but also because they generally separate terranes of different structural histories and strain pattern (e.g. Coward 1984). This interpretation has recently gained support from experimental rock deformation studies (Chopra & Paterson 1981, Shelton & Tullis 1981, Jaoult *et al.* 1984, Ranalli & Murphy 1987), which show that, with increasing stress, deformation tends to become localized (strain partitioning) into specific zones (mylonites).

As stated in the Introduction, the eclogitic shear zone is a km-scale zone that formed at a minimum depth of 40 km in a subduction zone and that was only locally overprinted by late-stage recovery processes and retrograde metamorphism. Thus, this shear zone is thought to have developed during burial or at least before the temperature peak of metamorphism. The shear zone contains 95–98% in volume of moderately to highly strained domains. These domains are characterized by an intense foliation and a marked grain size reduction (down to 5 μm). Thus, we suggest that the eclogitic shear zone developed during subduction zone metamorphism to subsequently act as a zone of detachment during a late stage of the Alpine orogeny. This is supported by the fact that, in the field, the eclogitic shear zone is bounded above by another major shear zone (or thrust contact) lined with metasediments and serpentinite bodies of different structural, kinematic and metamorphic histories. This latter shear zone was intensely deformed during blueschist and greenschist metamorphisms; it is interpreted as a second zone of high shear strain that nucleated on the mechanically weak eclogitic shear zone to subsequently accommodate displacement at the roof of the Lago Superiore unit during the rock exhumation history.

MODEL FOR OCEANIC CRUST DELAMINATION

In order to constrain if the oceanic lithosphere may undergo significant strength fluctuations in deep levels of subduction zones, a relevant rheological profile across a petrologically-stratified oceanic lithosphere subducted at 40 km depth has been constructed for a shear strain rate of 10^{-12} s^{-1} and an appropriate geothermal gradient of 12°C km^{-1} (Fig. 11). The diagram has been drawn assuming Byerlee's (1968) relation for friction in the thrust region (Sibson 1974) and using the flow law for steady-state creep of anorthosite, diopsidite (Shelton & Tullis 1981) and Åheim dunite (Chopra & Paterson 1981) of the form:

$$\frac{\tau}{G} = B^{-1/n} \cdot \dot{\gamma}^{1/n} \cdot \mathrm{e}\,(Q/RTn),$$

where τ is the shear stress, G is the shear modulus, B is a material constant, $\dot{\gamma}$ is the shear strain rate, Q is the activation energy, R is the gas constant, T is the temperature, and n is a material constant (see Ord & Hobbs 1989 for details).

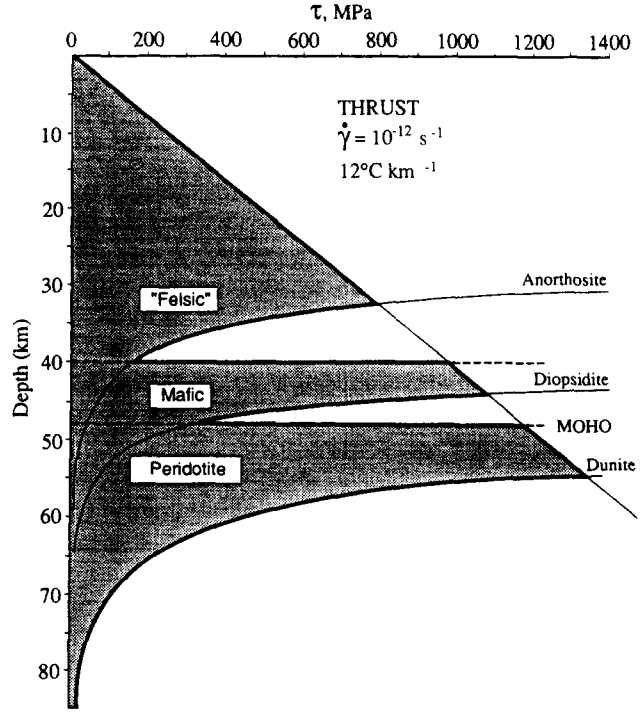

Fig. 11. Strength of the oceanic crust and upper mantle at 40 km depth in a subduction zone environment for thrust region with a geothermal gradient of 12°C km^{-1} and a shear strain rate of 10^{-12} s^{-1}. Plastic flow curve for anorthosite, diopsidite and dunite are shown (see text). For behaviour of thrust, rock density is 3.3×10^3 kg m^{-3}, coefficient of static friction (μ_s) is 0.75 and fluid pressure is hydrostatic. The thick line separating the blank from the dashed area represents a failure envelope.

Considering that omphacite controls the rheology of the oceanic crust below 40 km depth in a subduction zone environment and the 'wet' omphacite is a rheological equivalent diopsidite (our TEM study showed that both minerals have similar C2/c crystal symmetries), Figure 11 shows that a marked mechanical discontinuity should develop within a subducted oceanic crust at about 44–48 km depth. This implies that any rock type of appropriate chemical composition to form eclogite at a pressure of 12–14 kbar and a temperature of 500 ± 50°C should undergo intense crystal plastic flow, provided sufficient deviatoric stresses are present. From these, it is suggested that the km-scale eclogite ductile shear zone studied is best interpreted in terms of a major zone of delamination, which initiated within the eclogitized oceanic crust or close to the interface separating the uppermost mantle and the overlying oceanic crust during subduction. In addition, it should be emphasized that feldspar may have played a critical role in weakening the strength of the Fe-metagabbro at shallower depths during subduction. As shown in Fig. 11, the plastic flow curve of anorthosite intersects the Byerlee's relation for friction at about 33 km depth. This suggests that plagioclase, or at least breakdown reactions involving plagioclase (i.e. microcrystalline omphacite 1b) may have enhanced ductility in the Fe-metagabbro prior to accomplishment of eclogite facies equilibration; or in other words, that plagioclase controlled initial strain partitioning and associated weakening effects on a micro-scale in the reference metagabbro. This is in

agreement with our microstructural observations which show that, in the low strain rocks, plastic flow was primarily concentrated in the omphacite 1b domains.

CONCLUSIONS

(1) The microstructures preserved in the eclogitic tectonites studied indicate the operation of a wide range of deformation mechanisms that arises from a continuous variation both in time and space of (i) the internal morphology of the microstructures and (ii) the fluid content and location within different omphacite domains.

(2) Dislocation creep in omphacite is the dominant deformation mechanism, whereas (100) and (001) twinning, fracturing and fluid-phase diffusional creep are subordinate.

(3) Fracturing is interpreted in terms of brittle instabilities arising from strain and pore-fluid pressure partitioning between adjacent omphacite domains. Fluid phase diffusional creep caused omphacite precipitation in veins. The necessary fluid phase was progressively liberated by crystal plastic processes and subsequently trapped in veins. This process is cyclic in nature as the internally generated fluids can be released and trapped several times during progressive deformation.

(4) The km-scale eclogitic shear zone is interpreted as a mechanically weak zone that developed during burial or at least before the peak of temperature within a subducted oceanic crust at a minimum depth of 40 km. This zone of high shear strain subsequently acted as a zone of detachment during the Monviso exhumation history. This interpretation is in agreement with widespread recognition that, in zones of continental convergence, thin sheets of high pressure low temperature metabasic rocks occur lining the suture zones of orogenic belts.

Acknowledgements—H. L. M. van Roermund acknowledges receipt of a temporary research position at the Laboratoire de Pétrologie Métamorphique, Université de Paris 7. Collaboration with J. R. Kienast and his research group was indispensable in this respect. The kind hospitality of Madame Souchon contributed much to the realisation of this project. TEM analyses were preformed in the Laboratoire de Minéralogie Physique, CAESS, Université, de Rennes 1, and special thanks go to C. Willaime, P. Gillet and B. Reynard for their help and stimulating discussions. The paper has greatly benefited from careful reviews by R. Knipe and A. Ord. This work was supported by CNRS-INSU-DBT grant No. 4.10 "Fluides, minéraux et cinétique" to P. Philippot.

REFERENCES

Boudier, F. & Coleman, R. G. 1981. Cross section through the peridotites in the Samail ophiolite, Southeastern Oman. *J. geophys. Res.* **86**, 2573–2592.

Brodie, K. H. & Rutter, E. H. 1985. On the relationship between deformation and metamorphism, with special reference to the behaviour of metabasic rocks. In: *Metamorphic Reactions: Kinetics, Textures, and Deformation* (edited by Thompson, A. B. & Rubie, D. C.). *Adv. Phys. Geochem.* **4**, 138–179.

Buatier, M., Van Roermund, H. L. M., Drury, M. R. & Lardeaux, J. M. 1991. Deformation and recrystallisation mechanisms in naturally deformed omphacites from the Sesia Lanzo zone and its geophysical consequences. *Tectonophysics* **195** 11–27.

Byerlee, J. D. 1968. Brittle–ductile transition in rocks. *J. geophys. Res.* **73**, 4741–4750.

Caby, R., Kienast, J. R. & Saliot, P. 1978. Structure, métamorphisme et modèle d'évolution des alpes occidentales. *Rev. Geogr. phys. Géol. dyn.* **20**, 307–322.

Chopra, P. N. & Paterson, M. S. 1981. The experimental deformation of dunite. *Tectonophysics* **78**, 453–473.

Coward, M. P. 1984. Major shear zones in the Precambrian crust; examples from N.W. Scotland and southern Africa and their significance. In: *Precambrian Tectonics Illustrated* (edited by Kröner, A. & Greiling, R.). E. Schweitzerbart'sche Verlagsbuchhandlung, Stuttgart.

Dal Piaz, G. V., Hunziker, J. C. & Martinotti, G. 1972. La Zona Sesia-Lanzo e l'evolutione tettonico–metamorfica della Alpi Nord Occidentali interne. *Mem. Soc. geol. Ital.* **11**, 433–466.

Dewey, J. F. 1976. Ophiolite obduction. *Tectonophysics* **31**, 93–120.

Elter, G. 1971. Schistes lustrés et ophiolites de la zone piémontaise entre Orco et Doire Baltée (Alpes Graies). *Géol Alpine* **47**, 147–169.

Helmstaedt, H., Anderson, O. L. & Gavasci, A. T. 1972. Petrofabric studies of eclogite, spinel-websterite and spinel-lherzolite xenoliths from kimberlite-bearing breccia pipes in Southeastern Utah and Northeastern Arizona. *J. geophys. Res.* **47**, 4350–4365.

Ismail, I. A. H. & Murrell, S. A. F. 1976. Dilatancy and the strength of rocks containing pore water under undrained conditions. *Geophys. J. R. astr. Soc.* **44**, 107–134.

Jaoult, O., Tullis, J. & Kronenberg, A. K. 1984. The effect of varying contents on the creep behaviour of Heavitree quartzite. *J. geophys Res.* **89**, 4298–4312.

Kienast, J. R. 1983. La métamorphisme de haute pression et basse température (éclogites et schistes bleus): données nouvelles sur la pétrologie des roches de la croûte océanique subductée et des sédiments associés. Unpublished thèse d'Etat, University of Paris 6, Paris.

Kirby, S. H. & Kronenberg, A. K. 1984. Deformation of clinopyroxenite: evidence for a transition in flow mechanisms and semi-brittle behavior. *J. geophys. Res.* **89**, 3177–3192.

Kirby, S. H. & Kronenberg, A. K. 1986. Deformation of clinopyroxenite: reply. *J. geophys. Res.* **91**, 5027–5028.

Knipe, R. J. 1989. Deformation mechanisms-recognition from natural tectonics. *J. Struct. Geol.* **11**, 127–146.

Lardeaux, J. M., Caron, J. M., Nisio, P., Pequignot, G. & Boudeulle, M. 1986. Microstructural criteria for reliable thermometry in low-temperature eclogites. *Lithos* **19**, 187–203.

Lombardo, B., Nervo, R., Compagnoni, R., Messiga, B., Kienast, J. R., Mevel, C., Fiora, L., Piccardo, G. B. & Lanza, R. 1978. Osservazioni preliminari sulle ofiolite metamorfiche del Monviso (Alpi Occidentali). *Rend. Soc. It. Miner. Petr.* **34**, 253–305.

Monié, P. & Philippot, P. 1989. Mise en évidence de l'âge Eocène moyen du métamorphisme de haute pression dans la nappe ophiolitique du Monviso. (Alpes occidentales) par la méthode ^{39}Ar–^{40}Ar. *C. r. Acad. Sci., Paris* **309**, 245–251.

Nadeau, S., Philippot, P. & Pineau, F. In press. Fluid inclusion and mineral isotopic compositions in eclogitic rocks as tracers of local fluid migration in a subduction zone. *Earth Planet. Sci Lett.*

Nicolas, A. 1989. *Structures of Ophiolites and Dynamics of Oceanic Lithosphere.* Kluwer, Dordrecht.

Nicolas, A. & Le Pichon, X. 1980. Thrusting of young lithosphere in subduction zones with special reference to structures in ophiolitic peridotites. *Earth Planet. Sci. Lett.* **46**, 397–406.

Ord, A. & Hobbs, B. E. 1989. The strength of the continental lithosphere, detachment zones and the development of plastic instabilities. *Tectonophysics* **158**, 269–289.

Paterson, M. S. 1978. *Experimental Rock Deformation: The Brittle Field.* Springer, Berlin.

Philippot, P. 1987. Crack–seal vein geometry in eclogitic rocks. *Geodinamica Acta* **3**, 171–181.

Philippot, P. 1988. Déformation et éclogitisation progressives d'une croûte océanique subductée: l'exemple du Monviso, Alpes occidentales. Contraintes cinématiques durant la collision alpine. (Ph.D. thesis, University of Montpellier.) *Docum. Travaux Centre Géol. Géophys.* **19**, 1–269.

Philippot, P. & Kienast, J. R. 1989. Chemical-microstructural changes in eclogite-facies shear zones (Monviso, Western Alps, north Italy) as indicators of strain history and the mechanism and scale of mass transfer. *Lithos* **23**, 179–200.

Philippot, P. & Selverstone, J. 1991. Trace-element-rich brines in

eclogitic veins: implications for fluid composition and transport during subduction. *Contr. Miner. Petrol.* **106**, 417–430.
Post, R. L. 1977. High temperature creep of Mt Burnet dunite. *Tectonophysics* **42**, 75–110.
Raj, R. & Chyung, C. K. 1981. Solution–precipitation creep in glass ceramics. *Acta metall.* **29**, 159–166.
Ranalli, G. & Murphy, D. C. 1987. Rheological stratification of the lithosphere. *Tectonophysics* **132**, 281–295.
Rubie, D. C. 1983. Reaction-enhanced ductility: role of solid–solid univariant reactions in deformation of the crust and mantle. *Tectonophysics* **96**, 331–352.
Rubie, D. C. 1990a. Mechanisms of reaction-enhanced deformability in minerals and rocks. In: *Deformation Processes in Minerals, Ceramics and Rocks* (edited by Barber, D. J. & Meredith, P. G.). Unwin Hyman, London.
Rubie, D. C. 1990b. Role of kinetics in the formation and preservation of eclogites. In: *Eclogite Facies Rocks* (edited by Carswell, D. C.). Blackie, Glasgow, 111–140.
Ruff, L. & Kanamori, H. 1983. Seismic coupling and uncoupling at subduction zones. *Tectonophysics* **99**, 99–117.
Ruff, L. & Kanamori, H. 1988. Introduction to subduction zones. In: *Subduction Zones Part* 1 (edited by Ruff, L. & Kanamori, H.). *Pure & Appl. Geophys.* **128**, 449–453.
Rutter, E. H. 1972. The influence of interstitial water on the rheological behaviour of calcite rocks. *Tectonophysics* **14**, 13–33.
Rutter, E. H. & Brodie, K. H. 1988. The role of tectonic grain size reduction in the rheological stratification of the lithosphere. *Geol. Rdsch.* **77**, 295–308.
Schmid, S. M. & Casey, M. 1986. Complete fabric analysis of some commonly observed quartz axis pattern. In: *Mineral and Rock Deformation: Laboratory Studies* (edited by Hobbs, B. E. & Heard, H. C.). *Am. Geophys. Un. Geophys. Monogr.* **36**, 263–286.
Schutjens, P. M. 1991. Intergranular pressure solution in halite aggregates and quartz sands: an experimental investigation. (Ph.D. thesis, University of Utrecht) *Geol. Ultraiectina* **76**, 1–230.
Shelton, G. & Tullis, J. 1981. Experimental flow laws for crustal rocks. *Eos* **62**, 396.
Sibson, R. H. 1974. Frictional constraints on thrust, wrench and normal faults. *Nature* **249**, 542–544.
Spiers, C. J. & Schutjens, P. 1990. Densification of crystalline aggregates by fluid-phase diffusional creep. In: *Deformation Processes in Minerals, Ceramics and Rocks* (edited by Barber, D. J. & Meredith, P. G.). Unwin Hyman, London, 334–353.
Van den Beukel, J. 1990. Breakup of young oceanic lithosphere in the upper part of subduction zone: implications for the emplacement of ophiolites. *Tectonics* **9**, 825–844.
Van Roermund, H. L. M. & Boland, J. N. 1981. The dislocation substructures of naturally-deformed omphacites. *Tectonophysics* **73**, 403–418.
Weyl, P. K. 1959. Pressure solution and force of crystallization—a phenomenological theory. *J. geophys. Res.* **64**, 2001–2025.
White, S. H. 1976. The effects of strain on the microstructure, fabrics and deformation mechanisms in quartzites. *Phil. Trans. R. Soc. Lond.* **A238**, 69–86.
White, S. H. & Bretan, P. G. 1985. Rheological controls on the geometry of deep faults and the tectonic delamination of the continental crust. *Tectonics* **4**, 303–309.
White, S. H. & Knipe, R. J. 1978. Transformation- and reaction-enhanced ductililty in rocks. *J. geol. Soc. Lond.* **135**, 513–516.